A THERMAL MICROFLUIDIC ACTUATOR BASED ON A NOVEL MICROHEATER

*Dr. Nadeem Qaiser[§1**], Dr. Sherjeel M. Khan[1**], Dr. Wedyan Babatain[1], Dr. Maha Nour[1], Lana Joharji[1], Dr. Sohail F. Shaikh[1], Prof. Nazek Elatab[§1], and Prof. Muhammad Mustafa Hussain[§1, 2]*

[1] *King Abdullah University of Science and Technology (KAUST), Thuwal 23955, Saudi Arabia*

[2] *School of Electrical and Computer Engineering, Purdue University, West Lafayette, IN 47907, United States*

[**] *Equal contribution*

[§]*Corresponding Authors:*

mmhece@purdue.edu/muhammad.hussain@kaust.edu.sa
nazek.elatab@kaust.edu.sa
nadeem.qaiser@kaust.edu.sa

ABSTRACT

Microfluidic actuators based on thermally-induced actuation are gaining intense attraction due to their usage in disease diagnosis and drug release-related devices. These devices use a thermally-expandable polymer called Expancel that expands once its temperature exceeds a particular threshold value. Achieving such devices that are cost-effective and consume low input power is crucial for attaining efficacy. Therefore, the need for a low-energy consuming actuator necessitates the improved configurations of microheaters that provide the required heat. We report a novel topology of a copper-based microheater called square-wave meander, exhibiting a 44% higher output temperature, showing high actuation efficiency, as compared to the conventionally used meander design. The reason for increased temperature with low input energy is attributed to increased resistance by a jagged structure while maintaining the same surface area, i.e., without changing the effective thickness of the microheater. Numerical modeling demonstrates the comparison of temperature and electric potential contours for reported and conventionally used

microheaters. We reveal the merit of the reported design by comparing the volumetric thermal strains for both designs. We experimentally demonstrate the increased expansion of 25% for the reported design at the same applied current of 200 mA and faster operation time. Later, we show the microfluidic actuator device integrated into the microheater and PDMS-Expancel, controlling the operation/actuation of a fluid through a microchannel. This work might improve the performance of the advanced microfluidic-based drug release and other fluid-based applications.

Keywords: *microheater; thermal expansion; microfluidic actuator; FEM analysis; microchannel*

1. Introduction

In the area of personalized medicine, one of the major fields consists of the precise, fast, and cost-effective diagnosis of innumerable health problems. These diagnostic techniques base on numerous state-of-the-art technologies, including microfluidic systems. Such investigations mainly use the micro/nanoscale sample in the form of the fluids exerting pressure on them [1]. To analyze samples, flow control elements such as valves [2], mixers [3], and pumps [4] are gaining widespread attraction. For instance, microfluidic systems using micro-valve, micro-pump, and micro-injector, were used in protein/genomic analysis and bio-cells sorting devices [5–11]. Another compelling use of similar microfluidic systems is the controlled drug-delivery system that utilizes the micro-reservoir methods. The drug is temporarily stored in these reservoirs and then released to the desired locations, either in-vitro or otherwise, at a controlled rate [12–14]. These drugs can potentially cure ocular diseases and treat cancer cells etc. Generally speaking, these devices operate in a passive mode, i.e., the drug is released at a pre-planned rate and is usually irreversible [15]. Therefore, to acquire efficient and smooth operation, it is essential to comprehend the design, working mechanism, and physical significance of these devices.

The working mechanism of these devices depends on how we actuate or control the stream of the fluid, which will then be analyzed in the integrated device. One of the techniques to control the

movement of fluid is to use thermal energy, i.e., devices operating on thermally-induced actuation by using various thermal-responsive polymers. A micro-injector using the thermally-expandable polymer was reported by Samel *et al.* [16]. Likewise, previous studies have shown the usage of numerous polymer-based actuators that adopt thermally-induced actuation for drug delivery systems [17–22]. The benefits of thermal actuators include controlling the required expansion digitally, i.e., via a phone app, since they are operated by the amount of electrical energy, no additional mechanical components, and high efficiency due to the absence of friction effects. Although dielectric elastomer actuators may provide the actuation, the amount of actuation is limited to the intrinsic material properties of the dielectric material. In contrast, the performance of thermal actuators can be fine-tuned by improving the layouts of the heater.

For such thermally-induced actuation systems, the main components include the Poly-DimethylSiloxane (PDMS), a thermally expandable polymer called Expancel, a heat source, and a microfluidic channel-reservoir system. High flexibility, permeability to oxygen, and easiness of operation of PDMS make it a suitable material for biological and various microfluidic systems [23–29]. Next, the Expancel is composed of micro-sized spherical particles, which expand up to 40-fold of their original volume when heated at a particular temperature. The required temperature for the PDMS-Expancel is provided by using the microheater that could be digitally controlled to regulate the sample of bio-cell or release the drug. Expancel is cost-effective and provides the same expansion at a particular constant temperature, i.e., repeatable. Moreover, the expansion ratio can be controlled by changing the proportions of the PDMS/curing agent/Expancel. Various geometrical designs such as meander, spiral, fan, and others, have been reported that provide the heat using the Joule's effect [30–32]. Regardless of the application of Expancel-based microfluidic systems, the design of a microheater for low input power actuation is crucial for efficient operation. Nevertheless, there are a few studies that reveal the role of the topology of the microheater on the performance of the microfluidic actuator. Therefore, there is room to layout an improved design of a microheater that

provides the set temperature consuming low input power for a microfluidic actuator. Another important factor that needs to be considered is associated fabrication cost of these microheaters-based applications. Fan has reported a detailed analysis of the costs of similar systems.[33] The examples of advanced methods that potentially could lead to lower cost are casting/molding, additive manufacturing, and Laser ablation. However, the concern would be how much accuracy or resolution of these micro sized samples we can achieve. Therefore, there is a need to use low cost and simple design-based devices that would essentially would not cost insignificant cost to the whole system.

Here, we report a novel topology of a meander-shaped microheater, which provides a high output temperature by consuming the low input power as compared to the conventionally used straight-meander counterpart. The reported design consists of a jagged topology or structure called the square-wave meander that offers high resistance to the flow of electrons resulting in a high temperature. We first compare the performance of the conventionally used straight and our proposed wave-square meander microheaters by using numerical modeling. We then fabricate the microheaters using copper (Cu) on the polyimide (PI) substrate and demonstrate their working experimentally. Results show that a square-wave meander microheater induces high temperature (i.e., 101 ˚C) as compared to a straight meander (i.e., 70 ˚C) at the onset of the same applied current of 200 mA. In other words, it enables the boost of heating, up to 44%, or an increase in corresponding actuation efficiency. Our reported design also shows faster operation time. Then, we fabricate a microfluidic actuator containing the components, i.e., the microchannel of Poly(methyl methacrylate) (PMMA) and PDMS-Expancel on the top of the microheater. The PDMS-Expancel provides mechanical displacement to actuate or dispense the fluid from the reservoir to the outlet of the microchannel. The expansion profile of PDMS-Expancel shows that the square-wave microheater results in a 25% higher volumetric expansion as compared to the counterpart for the same amount of input current. The reason for this enhanced volumetric expansion was corroborated by numerical results. Our reported actuating device may potentially be used as a low power-consuming component of the drug-

release units and other fluid-based applications.

2. Results and Discussions

Generally speaking, heat is generated in a given material by the resistance to the flow of electrons when subject to electric current. Our proposed square-wave design converts a straight line of the conventional meander-shaped microheater into a jagged structure so that more resistance is offered to the flow of electrons/current while preserving the covered surface area. The name of the square-wave meander depicts that it has square shapes along its boundary. Although resistance could alternatively be increased by decreasing the thickness of a given microheater. Usually, from the perspective of the manufacturing's feasibility, getting the minimal thickness of these structures is one of the constraints. For instance, the current manufacturing strategies of Cu are not likely to further reduce the thickness. Therefore, to improve resistance and output temperature with low-energy input, beyond that point, the reported method can be used. The reported method raises the resistance of the conventional meander structure without changing its thickness. The schematics of conventionally used straight meander and jagged structure-based square-wave meander are shown in figures 1a and 1b, respectively. The enlarged designs for both cases, along with their parameters, are shown in figures 1c and 1d. The thickness (t), height (h), and width (w) of square-wave are 10 μm, 730 μm, and 600 μm, respectively, as shown in figure 1.

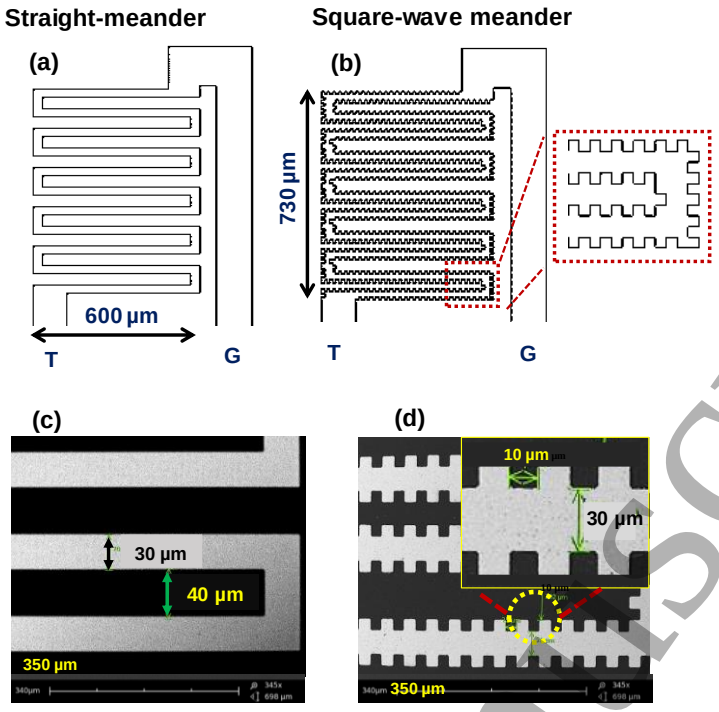

Figure 1. The straight and square-wave meander geometries of the microheater. *(a, b) Schematic diagram of straight and square-wave meander microheater (T: Terminal, G: Ground.). (c, d) SEM images of both microheaters with associated parameters, which reveal the topology of square-waves throughout the microheater coil. The size of the square is 10x 10 µm.*

Theoretically speaking, a given material could experience the temperature gradients, governed by the following equation (1):

$$Q = \rho C_p \frac{\partial T}{\partial t} - \Delta.(k.\Delta T) \qquad (1)$$

Here, ρ, C_p, T, k, and Q are density (Kg/m^3), heat capacity (J/K), temperature (K), thermal conductance (W/m.K), and heat source (J).

When an electric potential (V) is prescribed, resistive heating dictated by Joule's heating raises the temperature. Then, the generated heat follows the relation, given by equation (2):

$$Q = \varphi|\nabla V|^2 \qquad (2)$$

Whereas the φ represents the electrical conductivity (S/m) of the material, which can be related to the resistance ($R\ in\ ohm$)) by using $\varphi = \frac{1}{R}$. Also, we can relate the power consumed ($P\ in\ watt$) for a constant applied current (I) in ampere using the equation (3):

$$P = I^2R \quad (3)$$

Or for a constant applied potential, power consumed can be found by using equation (4):

$$P = \frac{V^2}{R} \quad (4)$$

Next, as the material under temperature gradients will experience thermal stress and strain, coupled thermal and elastic stress fields are used, as given by the following equations (5) and (6):

$$\varepsilon_{ij} = \frac{1}{2}\left(\mu_{i,j} + \mu_{j,i}\right), i, j = x, y, z \quad (5)$$

$$\varepsilon_{ij} = \frac{1}{E}\left[(1+\vartheta)\sigma_{ij} - (\vartheta I_1 - E\alpha\Delta T)\delta_{ij}\right], i, j = x, y, z \quad (6)$$

Whereas, ε_{ij}, $\mu_{i,j}$, E, ϑ, I_1, α, ΔT, and δ_{ij} are strain, displacement (m), Young's modulus (GPa), Poisson's ratio, stress invariant, coefficient of thermal expansion (m/m.K), temperature change, and Kronecker delta, respectively. The stress invariant is defined as $I_1 = \left(\sigma_{xx} + \sigma_{yy} + \sigma_{zz}\right)$.

We fabricate both of the Cu-based microheater designs on a PI sheet of 10 μm thickness. Figure 2 describes the fabrication process of the Cu microheater, the integration process of the PDMS with the reservoir, microchannel, and a fluid outlet, and the thermally expandable polymer (PDMS-Expancel) based microfluidic actuator. The detailed assembly process, i.e., the peeling process of PDMS, from the PMMA mold, containing the reservoir, microchannel, and fluidic outlet, and the assembly of the fully integrated actuator is shown in figure S1, video SMovie 1, and SMovie 2, in the supplementary information. This work will first demonstrate the benefits of the proposed design of a square-wave meander as compared to a conventionally used straight meander and then will employ the microheater for a practical actuating device, i.e., a microfluidic actuator. The detailed fabrication process from a microheater to a fully functional microfluidic actuator is described in the experimental details of the work.

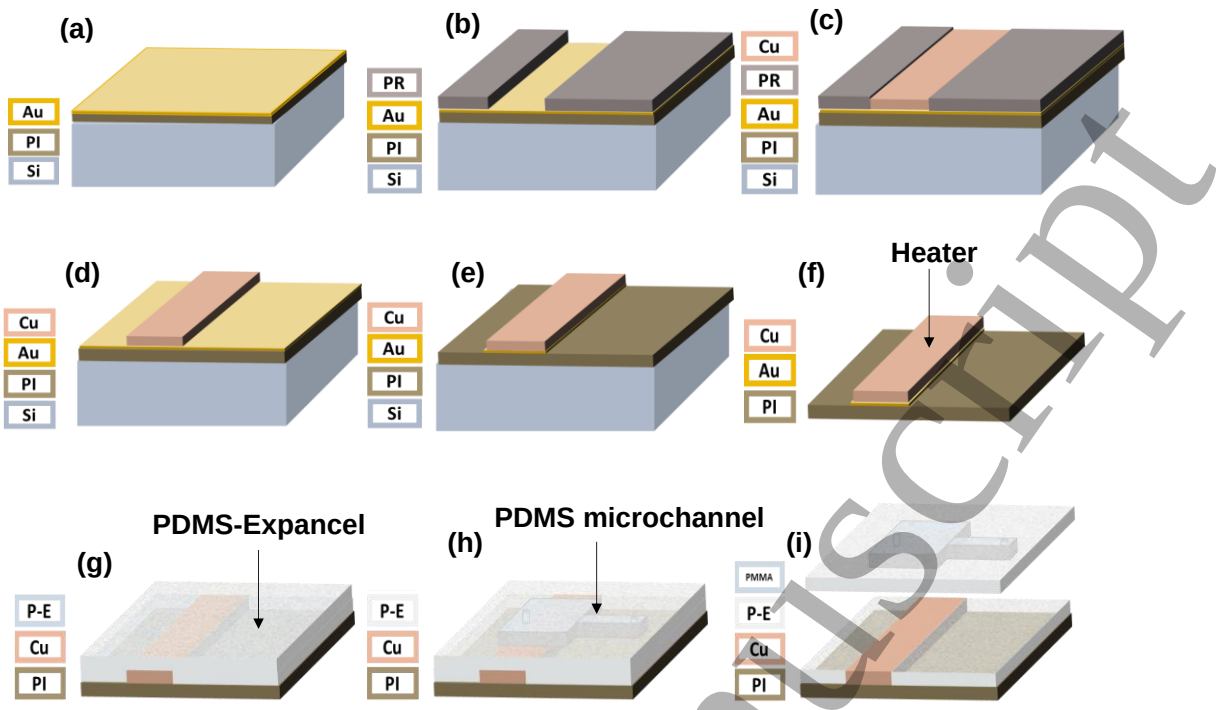

Figure 2. The fabrication process of the microheater and a thermal microfluidic actuator. *(a) Sputtering of 100nm Au, after spinning and curing of Polyimide (PI) of 10 µm on Silicon (Si) substrate. (b) Patterning of microheater by lithography and developing the photoresist (PR), (c) electroplating of copper of 4 µm using the input current of 0.105 A for 40 min, (d) removing the PR, (e) RIE etching of Au, and (f) manually peeling-off the PI from Si wafer. The integration of microfluidic devices on the microheater. (g) Spinning the PDMS-Expancel mixture, (h) fully assembled device with peeled PDMS from PMMA mold, microchannel integrated on the microheater, and (i) exploded view showing the full device with PMMA mold.*

To understand the response of the Cu-based microheater placed on top of the PI substrate, we numerically model both of the designs by using COMSOL™. The geometry of the structure and arrangement of materials is shown in figure S2a of supplementary information. The material properties of the Cu and PI are shown in table 1. For numerical calculations, the prescribed current on the terminal (T) was taken from 25 mA to 200 mA. The electric potential gradients of straight and square-wave meander microheaters are shown in figures S2b and S2c of supplementary information, respectively. Ohm's law dictates that electric potential changes linearly to the applied current, as shown in figure 3a. However, the magnitude of electric potential is higher for square-wave since it offers high resistance. The basic governing equations, as well as the results in figure 3a, exhibit that the output temperature of the square-wave meander microheater is expected to be higher as compared to the straight meander microheater. We map the output temperatures during the testing of

fabricated samples and compare the experimental results with numerical calculations. Figure 3b reveals the experimental temperature as a function of applied current and shows a good match with Finite Element Methods (FEM) calculations. As expected, the temperature of the square-wave meander microheater is higher as compared to the straight meander counterpart.

Now, for a given material, the temperature gradients produce the thermal strain and stress as provided by equations 5 and 6. It is worthy of mentioning that understanding of evolved thermal strains is crucial since we would place Expancel on top of the microheater and then employ the expansion of Expancel to actuate the microfluid, the details of which are discussed in the following sections. It is logical to state that mapping the real-time stress and strain in the Cu microheater by using experimental techniques would be difficult. Nevertheless, as experimental findings of temperature and potential gradients are well-matched with numerical calculations, we utilize the FEM modeling to calculate the von Mises stress (σ) and volumetric strain (ε_{vol}) in the microheater. Figures 3c and 3d show the evolution of maximum von Mises stress (σ_{max}) and ε_{vol} as a function of applied current. Figure S3 (a, c) of supplementary information demonstrates evolved strains, i.e., the amount of thermal strain (ε_{th}) and ε_{vol} in the straight meander microheater, and figure S3 (b, d) for square-wave meander microheater at the identical boundary conditions i.e. at the same amount of input current and thickness. As expected, the magnitude of the evolved strains for the square-wave is high due to the increased temperature. For reported devices, this might enhance the performance by providing a large expansion to the PDMS-Expancel layer that, in turn, improves the actuation of the microfluid for low power input. In other words, a square-wave microheater-based microfluidic actuator will provide high work output for the same amount of input energy as compared to the conventionally used straight meander counterpart.

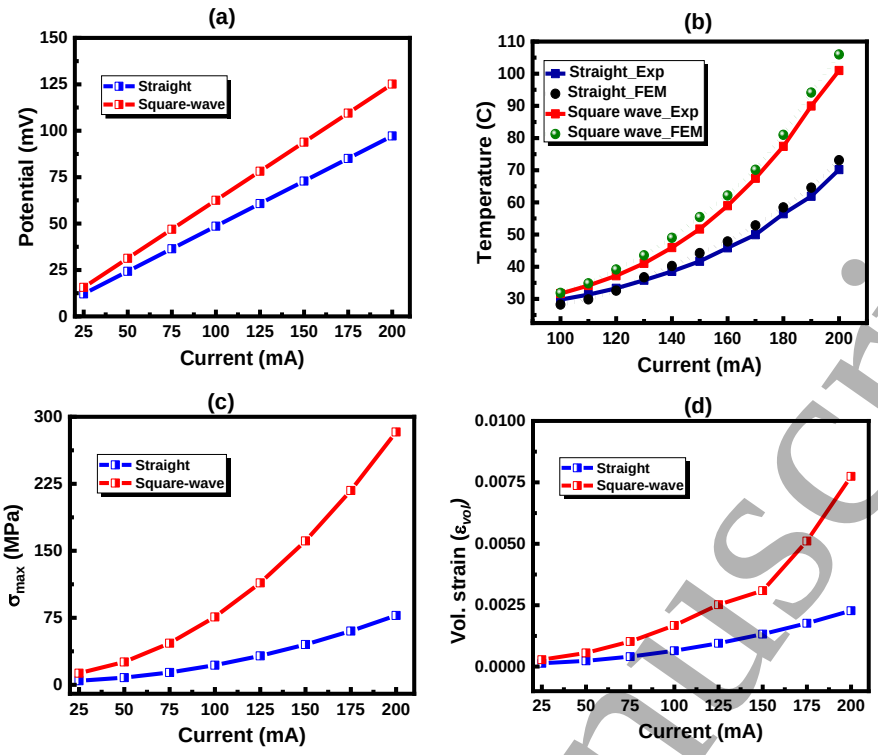

Figure 3. Comparison of experiments and numerical calculations for straight and square-wave meander microheaters. *(a) Numerical calculations of potential gradients, (b) numerical and experimental results of temperature contours showing that results matched very well to each other. Numerical calculations are showing the (c, d) maximum von Mises stress and volumetric strains for both designs.*

Next, we demonstrate the details of the temperature contours at a constant applied current. Figure 4 describes the results of temperature evolution by experimental and numerical calculations for both of the designs at a constant current of 200 mA. Figures 4a and 4b demonstrate the temperature contours by using numerical calculations. The 2D and 3D temperature gradients by experiments are shown in figure 4(c-f), respectively. Experimental results corroborate with FEM calculations showing that square-wave microheater yields high output temperature gradients for identical boundary conditions, i.e., same geometrical shape, parameters, and applied current. For instance, the maximum temperature for the square-wave structure is 101 ℃ as compared to 70 ℃ of a straight mender microheater, i.e., 44% higher for the comparable amount of input current. The reason for this increment is attributed to the high resistance offered by the jagged topology of the square-wave meander.

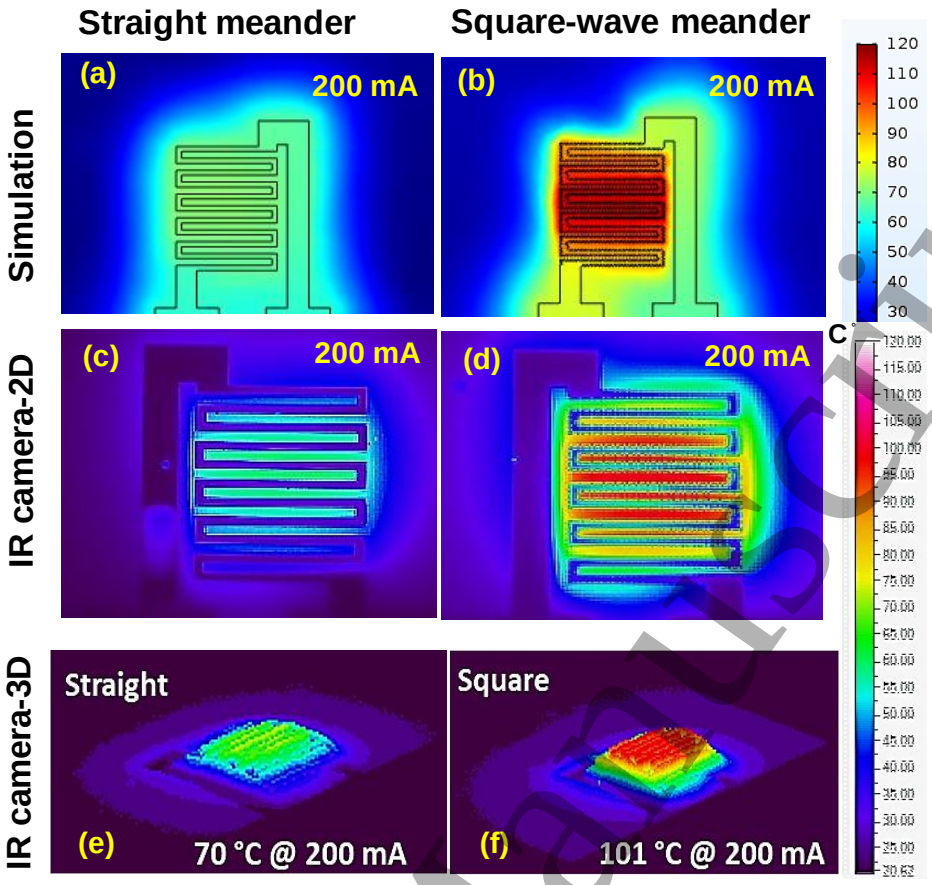

Figure 4. Evolution of temperature by FEM modeling and experiments for straight and square-wave meander microheaters. *At the onset of the applied current of 200 mA, FEM results showing (a, b) temperature contours for straight and square-wave microheater. Experimental validation by thermal IR camera, at the same boundary conditions showing the (c, d) 2D contours and (e, f) 3D contours of thermal gradients. Results show that for the identical areal coverage and prescribed boundary conditions, square-wave design produces a high temperature, i.e., 101 ˚C as compared to 70˚C for the straight meander.*

Figure 5 reveals the 3D stress and ε_{vol} contours for both of the microheaters by using the FEM calculations. As expected, the results show that the PI substrate does experience insignificant mechanical stress/strains; however, when compared, square-wave meander attains relatively high magnitudes of stress/strain. Moreover, mapping of volumetric strains for the same proves that a square-wave microheater will experience high tensile strain, and thus the polymer is expected to produce high expansion. The evolution of 3D contours is shown in vide SMovie 3 of the supplementary information.

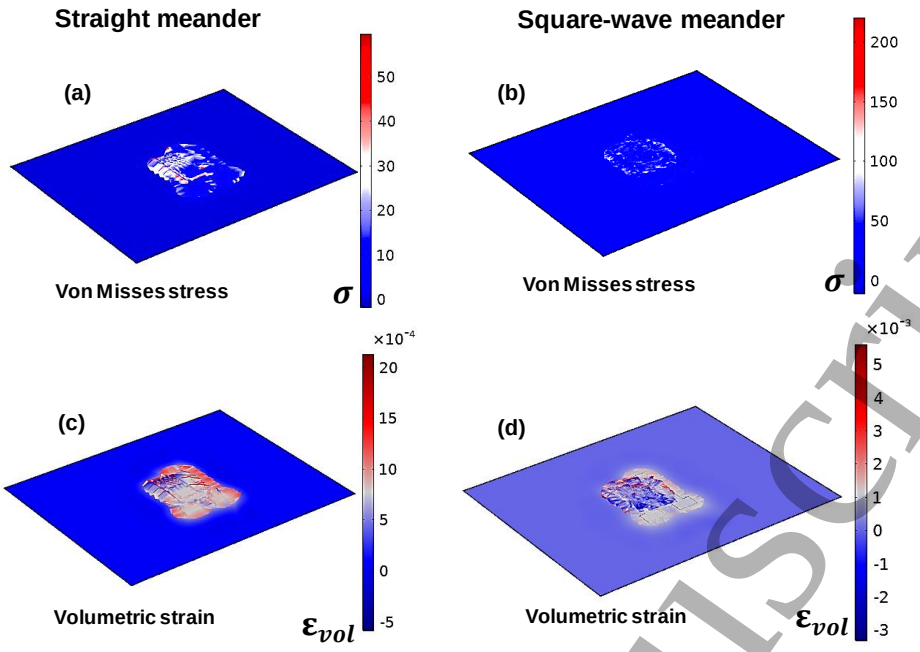

Figure 5. FEM modeling showing the 3D stress and strain contours at the onset of 200 mA. *(a, b) 3D stress contours (MPa) for straight and square-wave meander microheater showing the higher stress for square-wave since it experiences high temperature as compared to a straight one. (c, d) Mapping of volumetric strain for the same proving that square-wave microheater will experience high tensile strain, and thus the polymer is expected to produce high expansion.*

Now, moving forward, we take advantage of the reported jagged structure and essentially build a microfluidic actuator. The details of fabrication were given in experimental methods (shown in figure S1). We first configure the expansion profile of the PDMS-Expancel polymer and validate that amount of its physical expansion is high once placed at the top of the square-wave meander microheater. Figure 6a shows the initial state of the device that includes the PI/Cu/PDMS-Expancel structure. We then prescribe the current up to 200 mA and compare their expansion profile to reveal the merit of the reported design for the microfluidic actuator. Figures 6b and 6c reveal the expansion profiles of the PDMS-Expancel for straight and square-wave meander microheater-based devices, respectively. The time required to reach the final expansion, for the same input current, is called operation time and is one of the important features to consider for the stated device. Figure S4a and S4b exhibit that the reported design shows 3 times faster operation time. The reason is that for a conventional heater, the polymer takes a longer time to reach the threshold of getting the noticeable expansion, as shown SMovie 4. In contrast, the maximum attained temperature for square-wave swells the polymer in a shorter time due to higher values of temperature, shown in SMovie 5. The

details of the expansion profile are shown in SMovie 6 of the supplementary information. Interestingly, the expansion of PDMS-Expancel for square-wave is found to be large (10.5 mm) as compared to straight meander-based microheater (8 mm), showing a significant increase of 25%.

Lastly, we fabricate the fully-integrated actuator; figure 6d shows the optical image of the fluid reservoir, microchannel, and outlet. Figure 6e shows the fully integrated actuator utilizing the reported square-wave microheater in the stated device. The working of a microfluidic actuator is shown in figure 6f, indicating that the fluid was transported from the reservoir to the outlet promptly once the PDMS-Expancel expands and provides the required momentum to the microfluid. It is worth mentioning that due to non-linear relations, the expansion is slow at the start and becomes profound after reaching a certain temperature, therefore, 44% higher heating caused only 25% expansion. As our device aims for a one-time actuator/switch that would operate at a certain temperature, the stated fact would not affect the working of the microfluidic actuator. Our results suggest that the reported device offers a sufficient amount of actuation or controls/regulates the flow of fluid by consuming low input energy. For instance, for a specific period of battery-power input, our design provides increased heat in a given area. These sorts of devices are key components for drug-release and microfluid actuator-based units, and our design provides an efficient way to get high performance by using low power consumption.

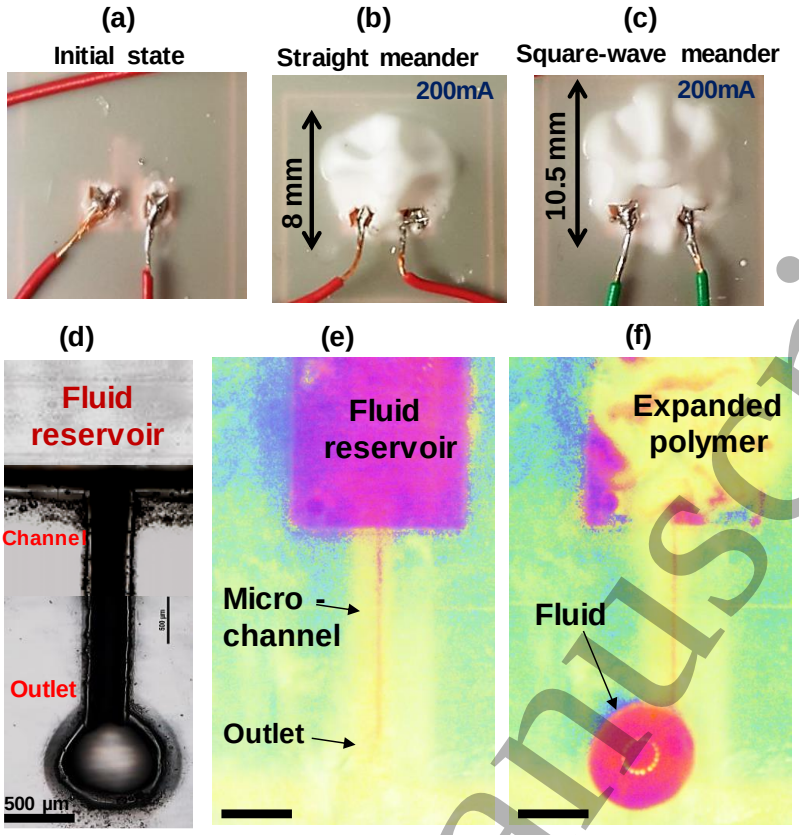

Figure 6: Expansion profile of PDMS-Expancel polymer and working of the microfluidic actuator. *(a) Initial state, i.e., showing no expansion in the polymer, (b, c) after applying the current of 200 mA. Results show that the expansion of polymer is higher when using a square-wave microheater showing the higher output/performance for the same consumption of current. Working of the microfluidic actuator based on integrated PDMS-Expancel polymer. (d) Optical image of a microchannel and fluid reservoir. (e) Top view of the fully integrated microfluidic actuator and (f) fluid control by actuation provided by expansion of PDMS-Expancel. The fluid was successfully released from a reservoir to the outlet passing through the microchannel. Scale bar = 500 µm*

3. Conclusions and Summary

In summary, we conduct numerical modeling and experiments to show the merits of the jagged topology of the square-wave meander microheater as compared to conventionally used microheater. We compare the expansion of PDMS/thermally-expandable polymer (PDMS-Expancel) for both cases and demonstrate the application in an efficient microfluidic actuator with a reported microheater. These results conclude that improving the microheater design while retaining a similar shape and covered area enables the enhancement of heating up to 44%, i.e., an increase in actuation efficiency. Numerical calculations reveal the comparison of thermal stress and volumetric strain of

both designs. Next, when we place the PDMS-Expancel layer on top of the square-wave microheater. We test and compared their volumetric expansion. Results show that the reported topology offers a 25% higher volumetric expansion, and three times faster operation time, in contrast to conventionally used microheaters. We also show the application of reported topology in a microfluidic actuator that can control or regulate the flow of a fluid in a microchannel. The proposed square-wave microheater, along with a microfluid actuator, could be a potential applicant in various microfluidic and bio-cells sorting and drug-release devices.

4. Materials and Methods

4.1 Numerical simulations

The electrical and mechanical simulations were conducted to display the electrical and corresponding mechanical response of straight and square-wave meander microheaters. The geometries of straight and square-wave meanders were designed by using the commercially available CAD tool Solidworks™. These designs were then imported to the commercially available Finite Element Methods (FEM) tool called COMSOL™ to perform the numerical calculations. The design of the PI substrate was built in COMSOL™, and then the imported model of microheater was assembled in the COMSOL™. Numerical analysis was performed using Joule's heating, and the range of applied current was chosen from 25 mA to 200 mA. To achieve the electric potential gradient, temperature distributions, and mechanical stress/strain, we used coupled modules of electric currents, heat transfer in solids, solid mechanics, and membrane. The electric currents were prescribed on one of the terminals (regarded as *T*) of the microheater, while the other was regarded as ground (*G*). The electrical conductivity of Cu, heat transfer coefficient and air temperature were taken to be 58.1 x 10^6 S/m, 20 W/(m^2. K), and 22.5 C $^{\circ}$, respectively. The thickness of the Cu microheater and PI substrate was taken as 4 μm and 10 μm, whereas the length and width of the PI substrate were considered as 50 mm and 40 mm, respectively. The convective heat flux was prescribed for calculating the temperature distributions when subject to electrical current. For

mechanics calculations, the bottom surface of the PI substrate was fixed, whereas the heating element of the microheaters and other surfaces were free to expand under thermal boundary conditions. We used a fine mesh on the heating coil and surrounding area to ensure the solution convergence. The material properties of Cu and PI are listed in Table 1.

Material	Size (h, w, t)-mm	Thermal conductivity-[W/m. K)]	Young's modulus-GPa	Poisson's ratio	Density-Kg/m^3
PI	50 x 40 x 0.01	0.12	3.1	0.34	1300
Cu	0.73 x 0.6 x 0.04	401	120	0.34	8960

Table 1. Material properties of Cu and PI

4.2 Fabrication and Characterization

First, we fabricated the straight and square-wave meander microheaters by using the flow described in Figure 2. To get PI of a thickness of 10 μm on the Si substrate, we performed the spinning at 2000 rpm for 30 sec. For curing of PI, we programmed the hot plate as follows: 90 C˚ for 90 sec, 150 C˚ for 90 sec, ramp to 320 C˚ with 240 C˚/hr, and was held at the same temperature of 320 C˚ for 30 min. A seed layer of gold (Au) of 100 nm thickness was sputtered on the PI. We designed the geometrical shapes of straight and square-wave meanders with respective width on a mask. After that, we performed patterning, using photolithography process EVG 620, and developing of photoresist (PR) for the design of Cu-based straight and square-wave meander shapes. Then, we did grow 4 μm of Cu by using electroplating. For electroplating, we set the current of 0.105 A and run the process for 40 min to get the required thickness. After the removal of PR, reactive ion etching (RIE) was used to remove Au. Then the PI from the Si wafer was manually peeled off.

To perform the integration of microfluidic devices on the microheater, we prepared a solution of PDMS-Expancel (a thermally expandable polymer). We took the ratio of PDMS: Curing Agent: Expancel to be 10:1:5, respectively. After degassing, we performed the spinning of PDMS-Expancel on the microheater. Lastly, we attained the PDMS-based microchannel, reservoir, and outlet,

utilizing the PMMA mold manufactured by the Laser ablation method, to get the fully integrated actuator based on the microheater. For experimental validation, a constant current ranging from 100 mA to 200 mA with an increment of 10 mA, was supplied by using a DC supply. The samples were placed under a thermal infrared (IR) microscope to observe the temperature changes. The temperature values were taken from the contour under an Infrared (IR) microscope. To ensure repeatability, we conducted a minimum of 5 experiments for each case. To capture the images at different stages of the experiment, we used a scanning electron microscope (SEM) and optical microscope.

Appendix A. Supplementary data

See supplementary material for the detailed microfluidic actuator device, FEM modeling schematic and FEM results of electric potential distribution, thermal and volumetric strain for a straight meander and square-wave meander microheaters, and operation time of PDMS-Expancel system. Supplementary material related to this article can be found online.

Availability of Data

The data that support the findings of this study are available from the corresponding author upon reasonable request.

Acknowledgment

This publication is based upon work supported by the King Abdullah University of Science and Technology (KAUST) Office of Sponsored Research (OSR) under Award No. REP/1/2707-01-01 and REP/1/2880-01-01.

Conflict of interests

We declare the authors have no competing financial/non-financial interests or other interests that might be perceived to influence the interpretation of the article.

Contributions

M. M. H. conceived the idea and directed the project; N.E directed the fabrication scheme, N. Q. conducted the experiments and simulations; S. M. K, and M.N and L. A assisted in the fabrication & testing and helped in the preparation of the manuscript, S. F. S. assisted in the heater fabrication, and W. B. helped in the testing of microfluidic structures.

REFERENCES

[1] Samel B, Nock V, Russom A, Griss P and Stemme G 2007 A disposable lab-on-a-chip platform with embedded fluid actuators for active nanoliter liquid handling *Biomed Microdevices* **9** 61–7

[2] Takao H, Miyamura K, Ebi H, Ashiki M, Sawada K and Ishida M 2005 A MEMS microvalve with PDMS diaphragm and two-chamber configuration of thermo-pneumatic actuator for integrated blood test system on silicon *Sens Actuators A Phys* **119** 468–75

[3] Nguyen N T, Huang X and Chuan T K 2002 MEMS-micropumps: A review *Journal of Fluids Engineering, Transactions of the ASME* **124** 384–92

[4] Iverson B D and Garimella S V. 2008 Recent advances in microscale pumping technologies: A review and evaluation *Microfluid Nanofluidics* **5** 145–74

[5] Easley C J, Karlinsey J M, Bienvenue J M, Legendre L A, Roper M G, Feldman S H, Hughes M A, Hewlett E L, Merkel T J, Ferrance J P and Landers J P 2006 A fully integrated microfluidic genetic analysis system with sample-in-answer-out capability *Proc Natl Acad Sci U S A* **103** 19272–7

[6] Jensen E C, Zeng Y, Kim J and Mathies R A 2010 Microvalve enabled digital microfluidic systems for high-performance biochemical and genetic analysis *JALA - Journal of the Association for Laboratory Automation* **15** 455–63

[7] Ma S, Murphy T W and Lu C 2017 Microfluidics for genome-wide studies involving next generation sequencing *Biomicrofluidics* **11**

[8] Matuła K, Rivello F and Huck W T S 2020 Single-Cell Analysis Using Droplet Microfluidics *Adv Biosyst* **4** 1900188

[9] Zhang Q, Wang T, Zhou Q, Zhang P, Gong Y, Gou H, Xu J and Ma B 2017 Development of a facile droplet-based single-cell isolation platform for cultivation and genomic analysis in microorganisms *Sci Rep* **7** 1–11

[10] Shen Y, Yalikun Y, Aishan Y, Tanaka N, Sato A and Tanaka Y 2020 Area cooling enables thermal positioning and manipulation of single cells *Lab Chip* **20** 3733–43

[11] Khater A, Abdelrehim O, Mohammadi M, Mohamad A and Sanati-Nezhad A 2021 Thermal droplet microfluidics: From biology to cooling technology *TrAC Trends in Analytical Chemistry* **138** 116234

[12] Stevenson C L, Santini J T and Langer R 2012 Reservoir-based drug delivery systems utilizing microtechnology *Adv Drug Deliv Rev* **64** 1590–602

[13] Lee H-P and Ryu W 2013 Wet microcontact printing (μCP) for micro-reservoir drug delivery systems *Biofabrication* **5** 025011

[14] Meng E and Sheybani R 2014 Micro- and nano-fabricated implantable drug-delivery systems: Current state and future perspectives *Ther Deliv* **5** 1167–70

[15] Lue S J, Chen C H, Shih C M, Tsai M C, Kuo C Y and Lai J Y 2011 Grafting of poly(N-isopropylacrylamide-co-acrylic acid) on micro-porous polycarbonate films: Regulating lower critical solution temperatures for drug controlled release *J Memb Sci* **379** 330–40

[16] Samel B, Griss P and Stemme G 2007 Active liquid aspiration and dispensing based on an expanding PDMS composite *2007 IEEE 20th International Conference on Micro Electro Mechanical Systems (MEMS)* (IEEE) pp 565–8

[17] Karimi M, Sahandi Zangabad P, Ghasemi A, Amiri M, Bahrami M, Malekzad H, Ghahramanzadeh Asl H, Mahdieh Z, Bozorgomid M, Ghasemi A, Rahmani Taji Boyuk M R and Hamblin M R 2016 Temperature-Responsive Smart Nanocarriers for Delivery of Therapeutic Agents: Applications and Recent Advances *ACS Appl Mater Interfaces* **8** 21107–33

[18] Chen Y Y, Wu H C, Sun J S, Dong G C and Wang T W 2013 Injectable and thermoresponsive self-assembled nanocomposite hydrogel for long-term anticancer drug delivery *Langmuir* **29** 3721–9

[19] Schmaljohann D 2006 Thermo- and pH-responsive polymers in drug delivery *Adv Drug Deliv Rev* **58** 1655–70

[20] Kashyap S and Jayakannan M 2014 Thermo-responsive and shape transformable amphiphilic scaffolds for loading and delivering anticancer drugs *J Mater Chem B* **2** 4142–52

[21] Chen G, Chen R, Zou C, Yang D and Chen Z S 2014 Fragmented polymer nanotubes from sonication-induced scission with a thermo-responsive gating system for anti-cancer drug delivery *J Mater Chem B* **2** 1327–34

[22] Zhou J, Pishko M V. and Lutkenhaus J L 2014 Thermoresponsive layer-by-layer assemblies for nanoparticle-based drug delivery *Langmuir* **30** 5903–10

[23] McDonald J C, Duffy D C, Anderson J R, Chiu D T, Wu H, Schueller O J A and Whitesides G M 2000 Fabrication of microfluidic systems in poly(dimethylsiloxane) *Electrophoresis* **21** 27–40

[24] Ng J M K, Gitlin I, Stroock A D and Whitesides G M 2002 Components for integrated poly(dimethylsiloxane) microfluidic systems *Electrophoresis* **23** 3461–73

[25] Sia S K and Whitesides G M 2003 Microfluidic devices fabricated in Poly(dimethylsiloxane) for biological studies *Electrophoresis* **24** 3563–76

[26] Unger M A, Chou H P, Thorsen T, Scherer A and Quake S R 2000 Monolithic microfabricated valves and pumps by multilayer soft lithography *Science (1979)* **288** 113–6

[27] Anderson J R, Chiu D T, Jackman R J, Chemiavskaya O, McDonald J C, Wu H, Whitesides S H and Whitesides G M 2000 Fabrication of topologically complex three-dimensional microfluidic systems in PDMS by rapid prototyping *Anal Chem* **72** 3158–64

[28] Becker H and Gärtner C 2000 Polymer microfabrication methods for microfluidic analytical applications *Electrophoresis* **21** 12–26

[29] Ha B H, Lee K S, Destgeer G, Park J, Choung J S, Jung J H, Shin J H and Sung H J 2015 Acoustothermal heating of polydimethylsiloxane microfluidic system *Sci Rep* **5**

[30] Bhowmick S, Iodice M, Gioffrè M, Breglio G, Irace A, Riccio M, Romano G, Grilli S, Ferraro P, Mecozzi L, Coppola S, Gennari O, Rega R and Coppola G 2017 Investigation of pyroelectric fields generated by lithium niobate crystals through integrated microheaters *Sens Actuators A Phys* **261** 140–50

[31] Chau C F and Melvin T 2012 Design and fabrication of a quasi-ordered nanoporous silicon membrane suitable for thermally induced drug release *Journal of Micromechanics and Microengineering* **22** 085028

[32] Lee S M, Dyer D C and Gardner J W 2003 Design and optimisation of a high-temperature silicon micro-hotplate for nanoporous palladium pellistors *Microelectronics J* **34** 115–26

[33] Fan Y 2018 Low-cost microfluidics: materials and methods *Micro Nano Lett* **13** 1367–72

Figure Legends

Fig. 1: The straight and square-wave meander geometries of the microheater.

Fig. 2: The fabrication process of the microheater and a thermal microfluidic actuator

Fig. 3: Comparison of experiments and numerical calculations for straight and square-wave meander microheaters.

Fig. 4: Evolution of temperature by FEM modeling and experiments for straight and square-wave meander microheaters.

Fig. 5: FEM modeling showing the 3D stress and strain contours at the onset of 200 mA.

Fig. 6: Expansion profile of PDMS-Expancel polymer and working of the microfluidic actuator.